Supporting Information

Amaral et al. 10.1073/pnas.1218087109

SI Materials and Methods

Molecular Dynamics Protocol. The molecular dynamics (MD) simulations were carried out using the program NAMD2 (1). Langevin dynamics was applied to keep the temperature (300 K) fixed. The equations of motion were integrated using a multiple time-step algorithm (2). Short- and long-range forces were calculated every 1 and 2 time steps, respectively, with a time step of 2.0 fs. Chemical bonds between hydrogen and heavy atoms were constrained to their equilibrium value. Long-range electrostatic forces were taken into account using the particle mesh Ewald (PME) approach (3), and the water molecules were described using the TIP3P model (4). The simulation used the CHARMM22-CMAP force field with torsional cross-terms for the protein (5) and the all-atom CHARMM36 force field for the phospholipids (6).

Simulating NavAb Structures Under Hyperpolarized-Membrane Conditions. With the purpose of performing structure-based gating-charge measurements (see below), each of the membrane-equilibrated NavAb structures NX^{++}, NX, NX^{-}, and NX^{--} was simulated under hyperpolarized-membrane conditions using a charge-imbalance protocol (7). In this scheme, the channel-membrane system is bathed in ∼100 mM NaCl salt concentration and air–water interfaces are then created at both sides of the membrane by extending the length of the simulation box in the direction perpendicular to the membrane. After a short equilibration of 1 ns run at constant volume, a transmembrane (TM) potential, ΔV, is imposed on the system by displacing Na^+ ions from one aqueous compartment to the other, while keeping the overall concentration of the bulk phases constant. Because the channel-membrane system behaves as a condenser, the imbalance q_0 between the electrolytes creates ΔV (Fig. S2). Production runs were performed at constant volume.

Electrostatic Potential. For a given system configuration j, the electrostatic potential $\Phi_j(\vec{r}, \Delta V)$ at position $\vec{r}$ was computed using the PME method as implemented in NAMD (8). In this scheme, the potential is obtained by solving Poisson's equation,

$$\nabla^2 \Phi_j(\vec{r}, \Delta V) = -4\pi \sum_i \rho_i(\vec{r}), \qquad \textbf{[S1]}$$

where ρ_i is the point charge approximated by a spherical Gaussian of inverse width σ_i and the summation runs over all atoms in the system. We considered a grid of 1.5 × 1.5 × 1.5 $Å^3$ and σ = 0.25 $Å^{-1}$.

Direct Measurement of Gating Charges. For a channel-membrane system, the voltage difference ΔV across the membrane is defined as $\Delta V = V_i - V_e$, with V_i and V_e, respectively, as the voltages of the internal and external membrane regions. In the present protocol, ΔV is related to the charge imbalance, q_0, between the electrolytes through $\Delta V = C^{-1} Q_0$. Here, Q_0 is the charge imbalance q_0 per membrane area A, that is, $Q_0 = A^{-1} q_0$. The quantity C is the membrane capacitance, which is constant for the channel-membrane system (9, 10), and q_0 can be written as $q_0 = q_i - q_e$, with q_i and q_e being, respectively, the net charge within the internal and external regions of the system. Note that q_0 results from contributions from protein charges and ions in solution, $q_0 = q_0^{protein} + q_0^{ion}$ and, accordingly, we can relate $q_0^{protein}$ to ΔV through $q_0^{protein} = -q_0^{ion} + AC\Delta V$. This allows us to compute the gating charge (Q) associated with two conformational states of the channel λ_1 and λ_2 as

$$Q = -\frac{1}{2}\left[q_0^{protein}(\lambda_2) - q_0^{protein}(\lambda_1)\right] \qquad \textbf{[S2]}$$

with $q_0^{protein}(\lambda_2)$ and $q_0^{protein}(\lambda_1)$ being the charge imbalance due to protein charges in theλ_1 and λ_2 conformations, respectively.

Here, for each of the membrane-bound NavAb structures NX^{++}, NX, NX^{-}, and NX^{--}, the electrostatic potential, $\Phi_j(\vec{r}, \Delta V)$, was calculated as an average over $n = 100$ system configurations sampled along 1 ns of a hyperpolarized-membrane simulation, that is,

$$\Phi(\vec{r}, \Delta V) = \frac{1}{100} \sum_{j=1}^{100} \Phi_j(\vec{r}, \Delta V). \qquad \textbf{[S3]}$$

The average of $\Phi_j(\vec{r}, \Delta V)$ over x and y provides the electrostatic potential profile Φ_z along the membrane normal (Fig. S2), and the difference between the Φ_z values at the two electrolyte regions of the systems provides the estimate of ΔV; as a reference, Φ_z was set to zero in the upper electrolyte. Finally, by considering Eq. **S2**, we compute the gating charge associated with each of the NavAb structures by considering the channel conformation NX^{++} as the reference structure (Table S3). Here, we compute q_0^{ion} relative to the center of the bilayer and consider the membrane capacitance estimated for a channel-membrane system, that is, C = 0.9 × 10^{-22} C·V^{-1}·$Å^{-2}$ (9); ΔV corresponds to the voltage estimated from the average over a simulation time window of 1 ns.

Conformational Analysis of Voltage-Sensor Domains and Pore Domains. The values of the two generalized coordinates, R ($NavAb$, VSD; t) = R and R ($NavAb$, PD; t) = P were computed along the MD trajectory using the formula

$$R(NavAb, l; t) = [D(KR, l, KA, l) + D(NavAb, l, KR, l; t) - D(NavAb, l, KA, l; t)]/2\, D(KR, l, KR, l), \qquad \textbf{[S4]}$$

where D (KR, l, KA, l) is the rmsd between the distance matrices of domain l in the activated-open (KA) and resting-closed (KR) structures. D ($NavAb$, l, KR, l; t) and D ($NavAb$, l, KA, l; t) are the rms deviations between the instantaneous distance matrix of domain l in NavAb and the corresponding matrices of KA and KR, respectively. Distance matrices are defined as M_{ij} ($NavAb$, l; t) = r_{ij} ($NavAb$, l; t), where l is the domain considered ($l \in \{VSD, PD\}$) and r_{ij} is the distance between the geometrical centers of the charged moiety of a given S4 residue ($j \in \{R_1, R_2, ..., R_4\}$) and the charged moiety of a given negatively charged or polar group ($i \in \{B_1, B_2, ..., B_6\}$). For the pore-domain (PD) distance matrix, we consider three PD-lining residues in the S6-helix bundle ($i, j \in \{F_1, F_2, F_3\}$); r_{ij} is the C_α–C_α average distance between nonadjacent subunit (i, j) pairs.

Sampling Selected Voltage-Sensor Domain Conformations. The present procedure consisted of applying a biased and an equilibrium MD simulation to the membrane-bound NavAb structure, NX, to guide it to a given R value and then relaxing the structure at that conformational distance without constraints. Note that the PD structure is also unconstrained. Three independent trajectories were generated, sampling NavAb conformations at R = 0.85 ± 0.02, 0.38 ± 0.06, and 0.14 ± 0.01 [average values over the four voltage-sensor domain (VSD) subunits]. The final membrane-equilibrated structures obtained from these simulations

are referred to as NX^{++}, NX^{-}, and NX^{--}, respectively. In detail, the biasing part of the MD simulation sampling the NavAb conformation at R = 0.85 ± 0.02 was accomplished as follows. The voltage sensors of NX and KA were first superposed, taking into consideration the main-chain atoms of the binding sites B_2 through B_5. A set of harmonic constraints, with a magnitude of 4.5 kcal·mol^{-1}·Å^{-2} and a velocity of 0.25 Å/ns, was then applied on the C_α and the side-chain atoms $H_2N = C_\zeta(NH_2)—N_\varepsilon H—C_\delta H_2$ of the S4 basic residues of NX, pulling the four VSDs toward KA until the channel reached the target conformational distance; the C_α atom positions of the protein's negatively charged binding sites B_2 through B_5 were fixed by harmonic constraints during the procedure. By pulling the NX VSD structures toward KR, we followed the same protocol to sample the NavAb conformation at R = 0.38 ± 0.06 and 0.14 ± 0.01. After the initial biasing step, the harmonic constraints are slowly released (over ∼4 ns) from the N to the C terminus of the protein. The equilibrium regime was achieved after relaxation of the channel structure for ∼30 ns, without any applied constraints (Fig. S1).

Sampling Selected PD Conformations. In two independent MD simulations, the PD-closed structures NX and NX^{++} were first biased toward an open-PD conformation (P ∼ 0.9) and then submitted to relaxation without any constraints for ∼30 ns. The final membrane-equilibrated structures obtained from these MD runs are labeled NX^{PO} and NX^{O}, respectively. In these simulations, by considering the main-chain atoms of residues F_1 through F_3 (Table S1) of NX and NX^{++} superposed on KA, the structure of NavAb was pulled toward KA by applying harmonic constraints (4.5 kcal·mol·$^{-1}$Å^{-2} and 0.25 Å/ns) on the C_α atoms of residues F_1 through F_3, while constraining the VSD and the S4–S5 linker at their reference NX or NX^{++} configuration; each pulling procedure lasted until the target conformational distance of ∼0.9 was reached. After the initial step, the channel was equilibrated following the same protocol as for sampling NavAb conformations along R, that is, annealing (∼4 ns) plus unconstrained equilibration (∼30 ns).

Structural Analysis of PD. We analyzed the pore-radius profiles of the final structures resulting from the equilibration runs for NX^{O} and NX^{PO}. As expected, NX^{PO} shows an intermediate character compared with NX^{O} and NX. Indeed, the radius of the pore at the constriction region is ∼1.0, ∼2.0, and 3.0 Å for NX, NX^{PO}, and NX^{O}, respectively. Importantly, the constriction results from the close proximity of different residues in NX^{PO} and NX^{O}; the major constraining element is Met^{221} for the former and Ile^{217} for the latter.

Secondary Structure Content of the S4 Segment. To detect possible α- to 3_{10}-helix transitions in S4 occurring along the activation pathway, we analyzed the secondary structure content of the segment spanning residues 96–112 using STRIDE (11). Relative occupancies of each of the secondary structure states defined in STRIDE were computed by taking the average over the four subunits and over the molecular configurations sampled along the equilibrium part of the trajectory. Interestingly, the secondary structure content is significantly different across the states: in the central and C-terminal regions of S4, the 3_{10}-helix content is larger in NX^{++} than in NX, and almost absent in NX^{-} and NX^{--}. These results are consistent with those previously obtained for Kv1.2, which shows a larger 3_{10}-helix propensity only in the C-terminal region of S4 in the activated conformation. Transition to the resting-state conformation during deactivation causes S4 to refold into an α-helix. Importantly, all of the resting-state models of Kv1.2 proposed so far show S4 in an α-helix conformation.

1. Phillips JC, et al. (2005) Scalable molecular dynamics with NAMD. *J Comput Chem* 26 (16):1781–1802.
2. Izaguirre JA, Reich S, Skeel RD (1999) Longer time steps for molecular dynamics. *J Chem Phys* 110(20):9853–9864.
3. Darden T, York D, Pedersen L (1993) Particle mesh Ewald: An N·log(N) method for Ewald sums in large systems. *J Chem Phys* 98(12):10089–10092.
4. Jorgensen WL, Chandrasekhar J, Madura JD, Impey RW, Klein ML (1983) Comparison of simple potential functions for simulating liquid water. *J Chem Phys* 79(2):926–935.
5. MacKerell AD, Jr., Feig M, Brooks CL III (2004) Improved treatment of the protein backbone in empirical force fields. *J Am Chem Soc* 126(3):698–699.
6. Klauda JB, et al. (2010) Update of the CHARMM all-atom additive force field for lipids: Validation on six lipid types. *J Phys Chem B* 114(23):7830–7843.
7. Delemotte L, Dehez F, Treptow W, Tarek M (2008) Modeling membranes under a transmembrane potential. *J Phys Chem B* 112(18):5547–5550.
8. Aksimentiev A, Schulten K (2005) Imaging α-hemolysin with molecular dynamics: Ionic conductance, osmotic permeability, and the electrostatic potential map. *Biophys J* 88 (6):3745–3761.
9. Treptow W, Tarek M, Klein ML (2009) Initial response of the potassium channel voltage sensor to a transmembrane potential. *J Am Chem Soc* 131(6):2107–2109.
10. Stefani E, Toro L, Perozo E, Bezanilla F (1994) Gating of Shaker K^+ channels: I. Ionic and gating currents. *Biophys J* 66(4):996–1010.
11. Frishman D, Argos P (1995) Knowledge-based protein secondary structure assignment. *Proteins* 23(4):566–579.

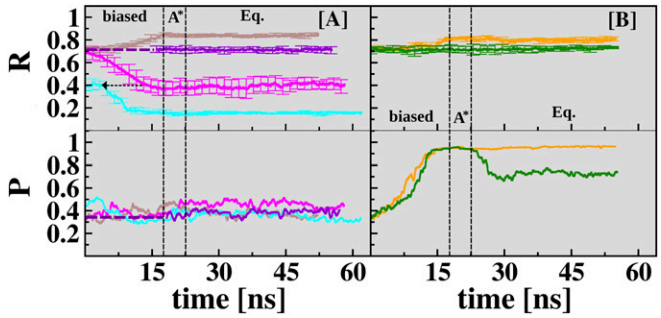

Fig. S1. Membrane-equilibrated conformations of NavAb. (*A*) *R* (*NavAb*, *VSD*; *t*) = R and *R* (*NavAb*, *PD*; *t*) = P profiles for the MD trajectories of the membrane-equilibrated NavAb conformations NX^{++} (brown), NX (violet), NX^{-} (magenta), and NX^{--} (cyan). Labels: biased, A*, and Eq. indicate, respectively, the biased, annealing, and equilibration phases of the MD trajectories. (*B*) As in *A* for the NavAb conformations NX^{O} (orange) and NX^{PO} (green). The profiles are computed according to Eq. 1; R profiles are averaged over the four channel subunits. Note the significant relaxation of P in the simulation, yielding the partially open channel structure, NX^{PO}. The equilibrium portion of the profiles is plotted in Fig. 1 to represent the projection of the MD trajectories onto the conformation-distance space {*R* (*NavAb*, *VSD*), *P* (*NavAb*, *PD*)}.

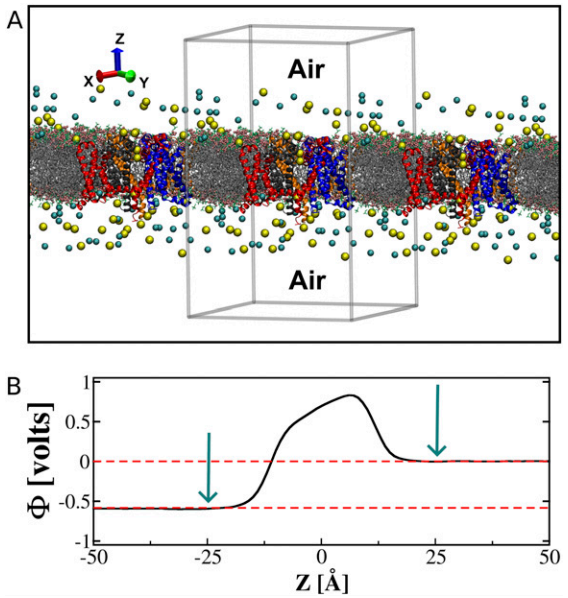

Fig. S2. Charge-imbalance simulation protocol enabling the application of a TM potential. (*A*) Cartoon illustrating a typical simulation setup of the channel embedded in a POPC (1-Palmitoyl-2-oleoylphosphatidylcholine) bilayer (licorice), surrounded by a 100 mM NaCl solution (Na in yellow, Cl in cyan, and water removed for visual clarity) and delimited by a pair of air–water interfaces along the *z* direction. The dimensions of the simulation box (gray) are x = 130 Å, y = 130 Å, and z = 300 Å. (*B*) Electrostatic potential profile along the bilayer normal, z of the channel-membrane system at hyperpolarized potentials. Φ_z is the average of $\Phi(r, \Delta V)$ over x and y coordinates. As a reference, Φ_z is set to zero in the upper electrolyte. In the present protocol, Φ_z shows plateau values in the aqueous regions (arrows). The red dashed lines define the applied voltage across the membrane bilayer. The difference between the plateau values at the two electrolytes corresponds to the TM potential ΔV.

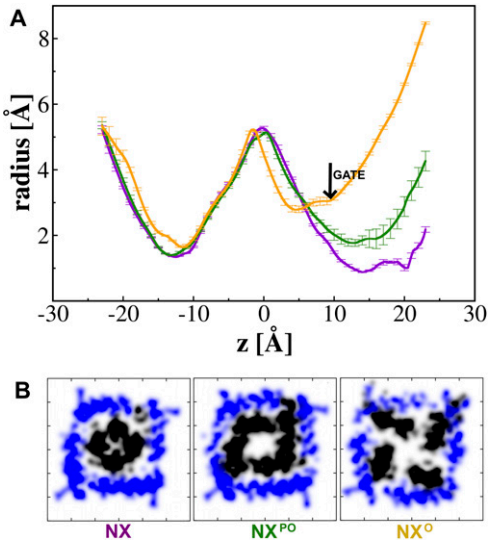

Fig. S3. (*A*) Pore-radius profiles along the lumen for NavAb conformations NX (violet), NX^{PO} (green), and NX^{O} (orange). The profiles are presented as a time average over the last 1 ns of the corresponding unconstrained MD trajectories. The radius at the most constricted region of the pore indicates a closed (~1.0 Å), partially open (~2.0 Å), and open (~3.0 Å) gate in conformations NX, NX^{PO}, and NX^{O}, respectively. The pore radius was calculated with HOLE (1). (*B*) Atomic-density plots for NX, NX^{PO}, and NX^{O} conformations, showing the position of the S4–S5 linkers (blue) and S6 helices (black) at the membrane plane placed at the intracellular entrance of the channel.

1. Smart OS, Goodfellow JM, Wallace BA (1993) The pore dimensions of gramicidin A. *Biophys J* 65(6):2455–2460.

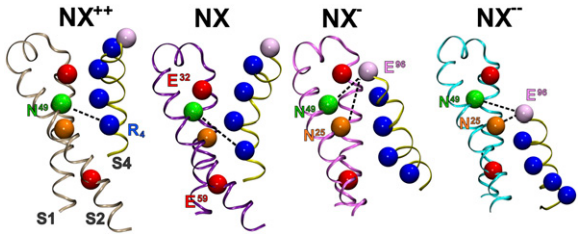

Fig. S4. Cartoons illustrating four conformations: NX^{++}, NX, NX^{-}, and NX^{--} of the NavAb VSD. Shown as spheres are C_β positions of key residues from helix S4: E^{96} (pink), R_1, R_2, R_3, and R_4 (blue), along with polar residues, N^{25} (orange), N^{49} (green), E^{32} (red), and E^{59} (red) from helices S2 and S1. For clarity, S1, S2, and S4 helices are drawn as ribbons. The dashed lines highlight spatial proximity between R_4 and N^{49} in conformations NX^{++} and NX and between E^{96} and N^{25}/N^{49} in conformations NX^{-} and NX^{--}.

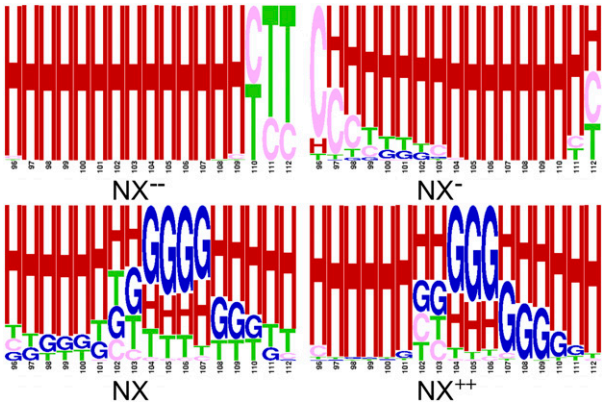

Fig. S5. The secondary structure content of S4 (residues 96–112) as defined by STRIDE (1) is shown for NX^{--}, NX^{-}, NX, and NX^{++}. Relative occupancies of each of the seven distinct states defining the secondary structure are computed by taking the average over the four subunits for all of the molecular configurations sampled during the equilibrium trajectories. Histograms were rendered with WebLogo (2) using the following labels and colors: α-helix (H, red), 3_{10}-helix (G, blue), coil (C, pink), and turn (T, green).

1. Frishman D, Argos P (1995) Knowledge-based protein secondary structure assignment. *Proteins* 23(4):566–579.
2. Crooks GE, Hon G, Chandonia JM, Brenner SE (2004) WebLogo: A sequence logo generator. *Genome Res* 14(6):1188–1190.

Table S1. Residues/groups considered for computation of the VSD and PD distance matrices

Channel	R_1, . . ., R_4*	B_1, . . ., B_6*	F_1, . . ., F_3
Kv1.2	R^{294}, R^{297}, R^{300}, R^{303}	PO_4^- (outer), E^{183}, E^{226}, D^{259}, E^{236}, PO_4^- (inner)	I^{402}, V^{406}, V^{410}
NavAb	R^{99}, R^{102}, R^{105}, R^{108}	PO_4^- (outer), E^{32}, N^{49}, E^{59}, D^{80}, PO_4^- (inner)	M^{209}, V^{213}, I^{217}
NavRh	R^{102}, R^{105}, R^{108}, R^{111}	PO_4^- (outer), N^{25}, D^{48}, E^{58}, D^{81}, PO_4^- (inner)	I^{211}, V^{215}, L^{219}

*For computation of the r_{ij} distances in the voltage-sensor distance matrix, the ij moieties correspond to the side-chain atoms $H_2N = C_\zeta(NH_2)—N_\varepsilon H—C_\delta H_2$ (Arg), $–OOC_\gamma—C_\beta H_2$ (Asp), $H_2N_{\delta 2}O\ _{\delta 1}C_\delta—C_\beta H_2$ (Asn), $–OOC_\delta—C_\gamma H_2$ (Glu), and the lipid phosphate group PO_4^-.

Table S2. Rmsd (Å) between NavAb and the reference structures KA, KR, and NavRh

	NX^{++}		NX		NX^-		NX^{--}	
Reference	S4	VSD	S4	VSD	S4	VSD	S4	VSD
NavRh	2.47 ± 0.99	2.55 ± 0.29	3.93 ± 0.12	3.25 ± 0.86	11.26 ± 1.46	6.08 ± 0.66	20.07 ± 1.21	10.43 ± 0.72
KA	3.59 ± 0.71	3.99 ± 0.17	4.48 ± 0.21	4.76 ± 0.10	8.36 ± 1.03	5.73 ± 0.20	16.74 ± 1.21	9.01 ± 0.49
KR	16.93 ± 0.94	9.19 ± 0.38	16.10 ± 0.64	9.00 ± 0.30	7.99 ± 1.62	5.98 ± 0.94	5.13 ± 0.92	4.11 ± 0.74

The rmsd values are estimates of the overall displacement of backbone segments of S4 and VSD. The rmsd values are calculated by superposing the acidic/polar binding sites within the VSD and are presented as averages over the four subunits.

Table S3. Direct measure of Q for the VSD conformations NX^{++}, NX, NX^-, and NX^{--}

Conformations	ΔV (volts)	Lipid area (Å^2)	q_0^{ion} (e)*	$q_0^{protein}$ (e)†	Q (e)‡
NX^{++}	−0.708	17309.1	−14	6.35	0
NX	−0.683	17229.9	−18	10.63	−2.14
NX^-	−0.674	16663.0	−30	22.99	−8.32
NX^{--}	−0.697	17251.8	−38	30.50	−12.08

*q_0^{ion} was computed relative to the center of the bilayer.
†Membrane capacitance $C = 0.9 \times 10^{-22}$ C·V^{-1}·A^{-2}; ΔV corresponds to the voltage estimated from the average over a simulation-time window of 1 ns.
‡Q was computed according to Eq. **S2** and considering NX^{++} as a reference.

Table S4. NavAb interatomic C_β–C_β average distances (Å) between S4 residues (E96 and R_1 to R_4) and the polar binding sites N25 and N49 from segments S1 and S2

Residue pairs	NX^{++}	NX	NX^-	NX^{--}
E^{96}-N^{25}	24.11 ± 1.22 (22.65)	22.57 ± 0.43 (21.87)	13.87 ± 1.24 (12.25)	8.66 ± 0.51 (8.06)
R_1-N^{25}	19.53 ± 0.96 (18.18)	17.16 ± 0.73 (16.11)	9.47 ± 0.82 (8.65)	8.88 ± 0.88 (7.68)
R_2-N^{25}	13.74 ± 1.03 (12.01)	11.69 ± 0.78 (10.61)	7.67 ± 1.11 (6.40)	13.31 ± 1.11 (11.90)
R_3-N^{25}	9.45 ± 0.26 (9.14)	6.49 ± 0.26 (6.05)	10.38 ± 1.50 (8.44)	18.56 ± 1.26 (16.86)
R_4-N^{25}	9.74 ± 0.54 (8.93)	8.36 ± 0.55 (7.72)	14.89 ± 1.99 (11.71)	22.78 ± 1.31 (20.95)
E^{96}-N^{49}	18.96 ± 1.32 (17.24)	19.69 ± 0.33 (19.13)	11.00 ± 1.70 (8.96)	11.38 ± 0.93 (10.15)
R_1-N^{49}	15.60 ± 1.11 (14.40)	14.14 ± 1.04 (12.47)	10.32 ± 1.33 (8.21)	13.98 ± 1.07 (12.67)
R_2-N^{49}	10.49 ± 0.82 (9.56)	10.02 ± 0.95 (8.89)	9.98 ± 2.05 (6.48)	19.21 ± 1.23 (17.52)
R_3-N^{49}	7.91 ± 0.61 (7.38)	9.08 ± 0.45 (8.62)	15.29 ± 1.46 (13.65)	24.62 ± 1.19 (23.08)
R_4-N^{49}	10.40 ± 0.53 (9.97)	13.70 ± 0.49 (13.03)	20.47 ± 1.38 (19.06)	29.32 ± 1.13 (27.86)

Pair distances are presented as averages over the four subunits; their minimum values are shown in parentheses.

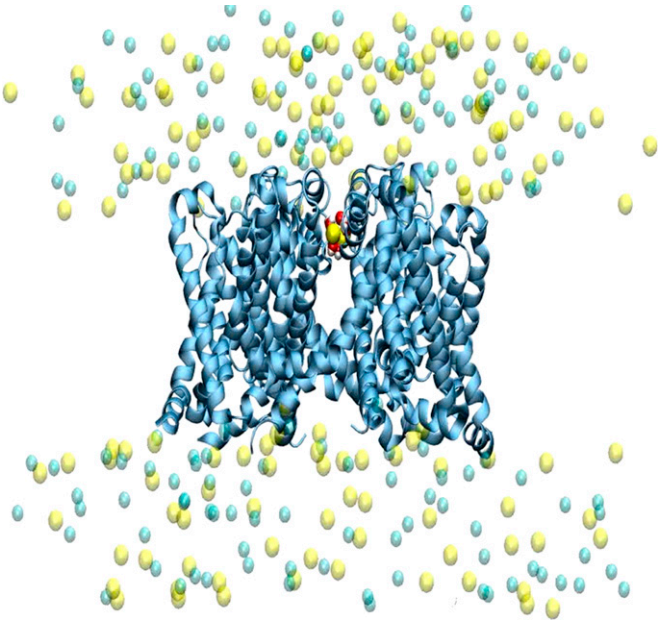

Movie S1. Short MD simulation under hyperpolarized-transmembrane conditions. The movie shows a conduction event of a fully hydrated Na^+ ion across the open activation gate of NavAb.

Movie S1

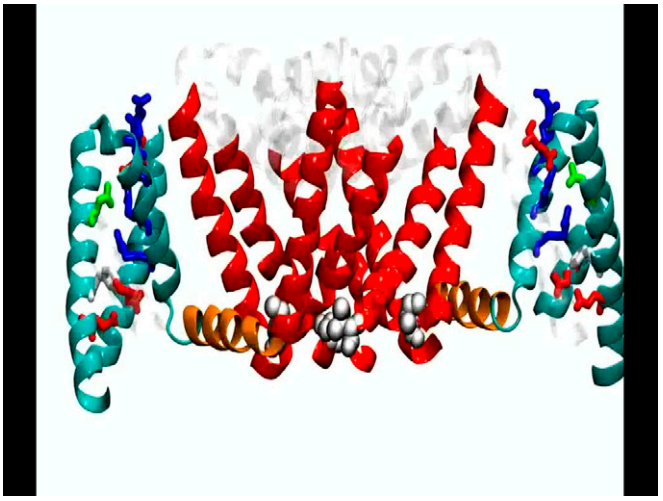

Movie S2. Sequential transitions of the NavAb sampled conformations from the activated-open (NX^O) to the resting-closed state (NX^{--}) of the channel. Only two subunits are shown for clarity. The VSD (cyan), S4–S5 linker (orange), and PD (red) are represented as cartoons; S4 arginines (blue), polar/acidic binding sites (green/red), and catalytic center residue F^{56} (white) are represented as sticks. The atoms of the hydrophobic gate residues I^{217} are rendered as silver spheres. Note the sequential slide of S4 arginines across the residue F^{56} and the hydrophobic collapse of residue I^{217}.

Movie S2